Multi-angle and non-uniform ground motions on cable-stayed bridges

Cite as:

Efthymiuo E, Camara A (2021) Multi-angle and non-uniform ground motions on cable-stayed bridges. Earthquake Spectra. Currently in press.

The definition of the spatial variability of the ground motion (SVGM) is a complex and multi-parametric problem. Its effect on the seismic response of cable-stayed bridges is important, yet not entirely understood to date. This work examines the effect of the SVGM on the seismic response of cable-stayed bridges by means of the time delay of the ground motion at different supports and of the loss of coherency of the seismic waves. The focus herein is the effect of the SVGM on cable-stayed bridges with various configurations in terms of their length and of design parameters such as the pylon shape and the pylon–cable system configuration, combined with the influence of the incidence angle of the earthquakes. The aim of this paper is to provide general conclusions that are applicable to a wide range of cable-stayed bridges, instead of attempting to interpret the effect SVGM on a case-by-case basis, and to contribute to the ongoing effort to interpret and predict the effect of the SVGM. It has been found that the effect of the SVGM on the seismic response of cable-stayed bridges varies depending on the pylon shape, height and section dimensions, on the cable-system configuration and on the response quantity of interest. Furthermore, the earthquake incidence angle defines whether the SVGM is important to the seismic response of the cable-stayed bridges. It is also observed that the SVGM excites vibration modes of the bridges that do not contribute to their seismic response when identical support motion is considered.

Keywords
spatial variability, cable-stayed bridges, pylon, incidence angle, incoherence effect, wave passage effect, higher-order modes

Introduction

Cable-stayed bridges are landmark structures that constitute key parts of transportation networks and are capable of spanning long distances that seemed impossible in the past. These structures are more flexible and light-weight than other bridge types with long vibration periods (Abdel-Ghaffar 1991; Abdel-Ghaffar and Khalifa 1991; Chen and Duan 2014), which means that they are subjected to lower spectral accelerations and lower seismic forces than stiffer bridge types. However, they also present lower damping values (less than the 5% of the critical damping that is commonly adopted) than other types of structures and hence, they are susceptible to dynamic loads such as wind and seismic loads (Kawashima et al. 1993). Furthermore, their extended length (which can reach several hundreds of meters in main span) suggests that their abutments and pylons are subjected to different ground motions because of the propagation of the earthquake with finite velocity, of the loss of coherency of the ground motion that reaches different supports and of the variable ground conditions that may be met among the abutments and the pylons; in other words the spatial variability of the ground motion (SVGM) is important.

The SVGM has been the topic of interest in the seismic response of bridges and long-span structures since the first dense instrument arrays were installed and started recording. Arrays such as the linear El Centro Differential Array which recorded the 1979 Imperial Valley, California earthquake (Spudich and Cranswick 1984), the two-dimensional Strong Motion Array in Lotung, Taiwan (SMART-1) (Bolt et al. 1982) and the three-dimensional Large Scale Seismic Test (LSST) also in Lotung (Abrahamson et al. 1991a,b) have provided engineers and seismologists with invaluable information on the SVGM.

The SVGM can result in the differential movement of the supports of structures that are extended in length. Eurocode 8; Part 2 defines the SVGM in bridges as a '*situation in which the ground motion at different supports of the bridge differs and, hence, the seismic action cannot be based on the characterisation of the motion at a single point*'. According to Abdel-Ghaffar (1991), the multi-support excitation begins when the structure is long with respect to the wavelengths of the input motion in the frequency range of importance to its earthquake response and consequently, different supports may be subjected to different excitations.

[1]Department of Civil and Environmental Engineering, Southern Methodist University, Dallas, TX
[2]School of Mathematics, Computer Science & Engineering, City, University of London, UK

Corresponding author:
Eleftheria Efthymiou, Ph.D., Department of Civil and Environmental Engineering, Southern Methodist University, Dallas, TX
Email: eefthymiou@smu.edu

In the case of cable-stayed bridges the SVGM results from the combination of three components (Der Kiureghian and Neuenhofer 1992; Der Kiureghian 1996); the wave passage effect which refers to the difference in the arrival times of the ground motion to different supports of the bridge (i.e. abutments, piers and pylons); the incoherence effect which refers to the loss of coherency of the ground motion due to consequent reflections and refractions of the seismic waves in heterogeneous soil media as they travel from the source to the bridge; and the site response effect which reflects the modification of the amplitudes and the frequency contents of the ground motions at the different supports of the bridge due to changes in the local site conditions in the vicinity of the foundations.

The effect of the SVGM on the structural response depends on a number of factors including the amplitude of the seismic motion, the incidence angle of the seismic waves relatively to the axis of the structure, the geometric characteristics of the structure and the stiffness of the surrounding soil. This effect has been examined in different types of multiply-supported and long structures (Hindy and Novak 1980; Abdel-Ghaffar and Rubin 1983; Lee and Penzien 1983; Luco and Wong 1986; Hao et al. 1989; Zerva 1990; Abdel-Ghaffar and Nazmy 1991; Zerva 1991; Hao 1997; Shinozuka et al. 2000; Soyluk and Dumanoglu 2000; Tzanetos et al. 2000; Chen and Harichandran 2001; Allam and Datta 2004; Sextos et al. 2004; Soyluk and Dumanoglu 2004; Sextos and Kappos 2009; Bi et al. 2010; Sextos et al. 2014; Papadopoulos et al. 2017; Efthymiou 2019; Efthymiou and Camara 2021, among others) and it has been found that the SVGM induces differential movements among the supports of such structures which modify their seismic response (Hao et al. 1989). The multi-support excitation results in the decrease of the inertia-generated forces in a structure when compared to the forces resulting from the identical motion of the supports, and at the same time it generates pseudo-static forces that are not present when identical support motion is considered (Priestley et al. 1996).

The wave propagation velocity can influence significantly the effect of the SVGM on the response of a long structure. Typically lower values of the propagation velocity tend to increase the structural response by increasing the pseudo-static forces induced under the SVGM and by decreasing their dynamic counterpart (Abdel-Ghaffar and Nazmy 1991; Zerva 1991; Soyluk and Dumanoglu 2000; Wang et al. 2003; Soyluk and Dumanoglu 2004; Bi et al. 2010). On the other hand, with increasing values of the wave propagation velocity the pseudo-static forces are reduced; and in the limit of an infinite value of the velocity of propagation the problem is reduced to the synchronous motion for which the pseudo-static effects are eliminated and the response is completely represented by the dynamic component (Soyluk and Dumanoglu 2000). Zerva (1991) investigated the impact of the incoherence and the wave passage effects on the response of multiply-supported structures by analysing two- and three-span continuous symmetric beams. The author concluded that the incoherence effect is more important than the wave passage effect, which can be neglected in cases where the seismic waves are highly incoherent. Shinozuka et al. (2000) verified that the incoherence effect is usually more important than the wave passage effect in typical highway bridges, but for longer spans, as the case of cable-stayed bridges, the time delay of the seismic motion at different supports may become critical. The flexibility of the foundation can also affect the impact of the seismic waves on the structure. The SVGM is closely linked with the interaction of the foundation

with the surrounding soil and the structure, most commonly referred to as soil–structure interaction or SSI (Lou and Zerva 2004; Sextos et al. 2004; Burdette et al. 2006).

The SVGM is more important on stiff structures and, typically, it does not significantly affect the response of longer and more flexible structures (Abdel-Ghaffar and Nazmy 1991; Nazmy and Abdel-Ghaffar 1992). The pseudo-static component of the structural response is responsible for the increased influence of the SVGM on stiff structures (Priestley et al. 1996; Zerva 2009), as opposed to flexible structures in which the total response is dominated by the dynamic component (Bi et al. 2010). This statement can be extended in the sense that the stiffer components of a structure such as a cable-stayed bridge that is composed of elements with very different flexibilities, are more vulnerable to the multi-support excitation.

Finally, the combination of the incidence angle with the SVGM has started to gain attention, with limited studies stating that the maximum value of the response quantity under consideration may not occur when the direction of propagation coincides with the principal axes of the bridge. Specifically, Allam and Datta (2004) and more recently Khan (2012) examined a 335-m span cable-stayed bridge with different orientations with respect to the propagation of the earthquake and subjected to ground motions whose rate of correlation depended on the incidence angle of the earthquake. The authors observed that there existed critical orientations of the examined bridge, which depended on the response quantity of interest and the region of the bridge under consideration, in which the structural response was larger than the obtained one when the ground motion coincided with the principal directions of the bridge.

The increasing number of cable-stayed bridges that are constructed in seismically active regions worldwide establishes the need to understand the seismic behaviour of these structures and especially of the pylons, which are responsible for the overall structural integrity of the bridge and whose seismic design usually governs their overall design in seismic prone regions (Duan 2012; Gimsing and Georgakis 2012). In these structures the multi-support excitation is undeniably linked with the seismic response and despite the existing studies, the effect of the SVGM is not entirely understood. The objective of this paper is to provide for the first time practical conclusions regarding the effect of the SVGM on the seismic response of cable-stayed on the basis of different engineering parameters such as the length of the bridge, the pylon shape and the pylon–cable system configuration, combined with the incidence angle of the earthquake. From the dynamic analysis of a large number of cable-stayed bridges with different configurations that are subjected to multi-angle and spatially variable ground motions it has been observed that the influence of the SVGM on the seismic response of the bridges is strongly affected by the shape of the pylons, the pylon–cable system configuration and by the incidence angle of the seismic waves. It has been found that the effect of the SVGM on the seismic response of cable-stayed bridges depends on the shape, height and section dimensions of the pylon, on the cable-system configuration and on the response quantity of that is examined. Furthermore, the earthquake incidence angle defines whether the SVGM is important to the seismic response of the cable-stayed bridges. Finally, the SVGM also excites vibration modes that do not contribute to the seismic response of the pylons when identical support motion is considered.

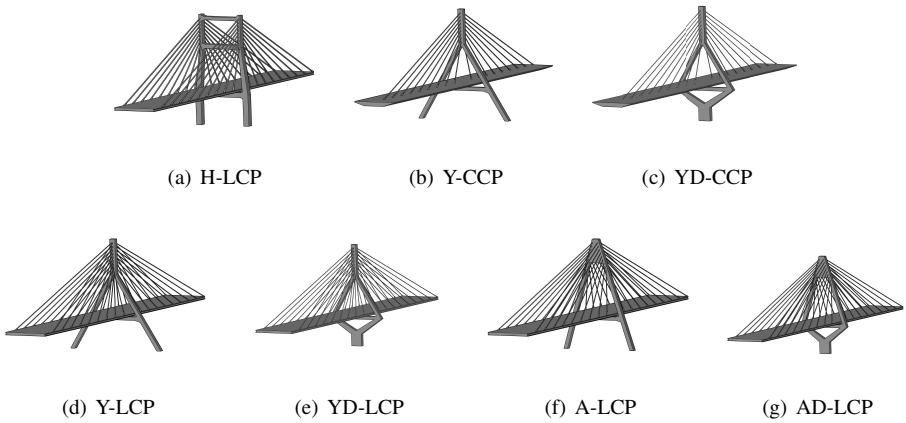

(a) H-LCP (b) Y-CCP (c) YD-CCP

(d) Y-LCP (e) YD-LCP (f) A-LCP (g) AD-LCP

Figure 1. Different pylon shapes and cable system arrangements considered in this work, along with the reference keywords. The part of the notation before the hyphen corresponds to the shape of the pylon. The letter 'D' stands for the lower diamond configuration which has been considered in the inverted 'Y'- and 'A'- shaped pylons. The cable arrangement is included in the second part of the notation after the hyphen and dictates two lateral cable planes (LCP) or one central cable plane (CCP).

Numerical Models

The bridge models of this study are the sequence of previous works from Camara (2011), Camara et al. (2014) and Efthymiou and Camara (2015). The overall arrangement of the bridges consists of two symmetric reinforced concrete pylons, a composite deck and the cable system. The length, L_P, of the main span, between the centres of the two pylons, takes values of 200, 400 and 600 m, representing short-span, intermediate-span and relatively long-span cable-stayed bridges, respectively. Pylons with conventional 'H', inverted 'Y' and 'A' shapes have been considered. A diamond configuration has also been adopted in the lower part of the pylons of inverted 'Y' and 'A' shapes, as shown in Fig. 1 wherein the notation of the pylons is also included and will be followed hereinafter. Altogether 21 bridge models have been considered.

The length of the main span, L_P, defines the length of the side spans, L_S, as shown in Fig. 2, and the number of cables, N_T, in each plane; $N_T = 9$, 19 and 29 when $L_P =$ 200, 400 and 600 m, respectively. The height of the pylons above the deck level, H, is also a function of L_P; $H = {}^{L_P}\!/_{4.8}$ and it is the same for all pylon shapes. Below the deck the height of the pylon is $H_i = {}^{H}\!/_{2}$, resulting in the total height of the pylon being $H_{tot} = H + H_i =$ 62.5, 125 and 187.5 m for the $L_P =$ 200-, 400- and 600-m bridges, respectively. The heights of the different parts of the pylons along with the section dimensions of the pylon legs and transverse struts are defined as functions of H (Camara et al. 2014).

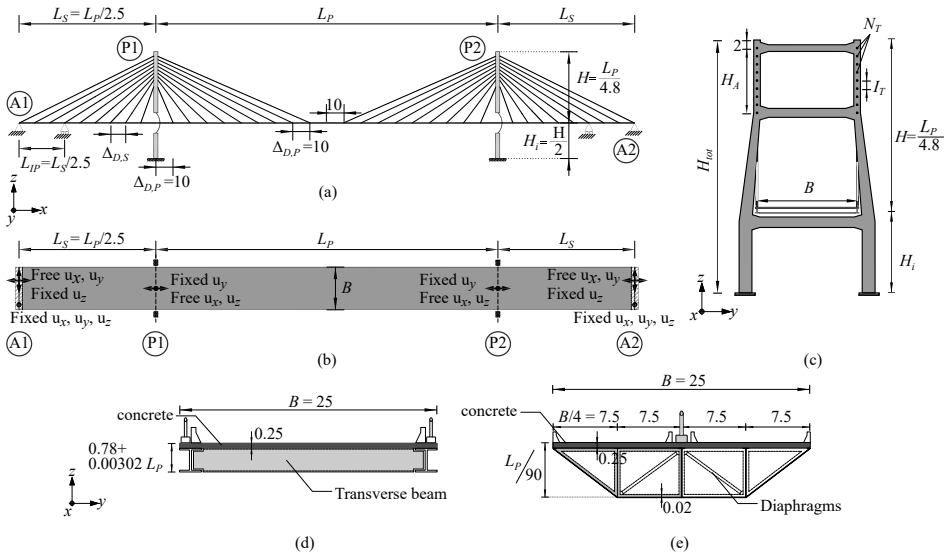

Figure 2. Parametric definition of the cable-stayed bridge models. (a) Complete bridge elevation, (b) complete bridge plan view, (c) sample 'H'-shaped pylon (the same parametrisation rules are applied to the inverted 'Y'- and 'A'-shaped pylons), (d) LCP deck, (e) CCP deck. All dimensions are in [m].

The cables are arranged in a semi-harp configuration in the orientation parallel to the traffic, whereas in the transverse direction two different configurations have been employed; two lateral cable planes (LCP) for all the pylon geometries and one central cable plane (CCP) only for the inverted 'Y'-shaped pylon with and without the lower diamond (see Fig. 1). Two different deck sections have been examined with shapes associated with the two cable system configurations. In the case of two LCP's the deck has an open section, as opposed to adopting a closed box section when one CCP is selected. The width of the deck is 25 m to accommodate four traffic lanes, regardless of the length of the bridge. In LCP models the deck has an open composite cross-section formed of two longitudinal I-shaped steel girders at the edges and a 25-cm thick concrete slab on top. To ensure the overall stability of the deck, transverse I-beams connecting the two longitudinal girders are placed at fixed intervals. In CCP bridges the deck is a composite box girder formed of a steel U-section closed by a 25-cm thick concrete slab that provides the bridge with sufficient torsional rigidity. The composite box section is stiffened with transverse steel diaphragms at the same fixed intervals as in the open deck section of the bridges with two LCP's. In the side spans vertical piers are placed at a distance of $L_{IP} = L_S/2.5$ from the abutments that constrain the vertical displacement of the deck in order to control the longitudinal displacement of the upper part of the pylon where the cable system is anchored (see Fig. 2).

Figure 2 shows that the abutments constrain the displacements of the deck in the vertical (z), transverse (y–perpendicular to the traffic flow) and longitudinal (x) directions and they also prevent its torsional rotation (θ_{xx}), whereas the rotations around the transverse (θ_{yy}) and the vertical axis (θ_{zz}) are released. In the side spans the intermediate piers constrain the vertical displacement and the torsional rotation of the deck. At the pylons the deck is restrained in the y direction and it is released in all other directions, assuming a floating type connection between the deck and the pylon which is commonly adopted in the design of cable-stayed bridges in seismic prone regions. The SSI is considered by replacing the soil around the foundation of the pylons with a system of springs and dashpots with stiffness and damping properties obtained from Gazetas (1991). For a harmonic excitation the dynamic impedance of the soil–foundation system is defined as the ratio between the force (or moment) and the resulting steady-state displacement (or rotation) at the centroid of the base of the massless foundation (Gazetas 1991):

$$\mathrm{S}_i = \frac{\mathrm{R}_i(t)}{\mathrm{U}_i(t)} \tag{1}$$

where $\mathrm{R}_i(t) = R_z \exp(\mathrm{i}\,\omega t)$ is a harmonic force (or moment) and $\mathrm{U}_i(t)$ is the resulting from $\mathrm{R}_i(t)$ steady-state displacement (or rotation) along the direction i of the excitation. Impedances S_i are computed herein for the longitudinal motion in the direction parallel to the traffic (S_x, longitudinal swaying), for the transverse motion perpendicular to the traffic (S_y, lateral swaying), for the vertical motion (S_z), for the rotational motion of the foundation about the longitudinal axis (S_{rx}, rocking) and for the rotational motion along the transverse axis (S_{ry}, rocking). For each direction the impedance is:

$$\mathrm{S} = \overline{K} + \mathrm{i}\,\omega C \tag{2}$$

in which $\overline{K}$ and C are functions of the circular frequency ω. The real component $\overline{K}$ of the complex Eq. (2) is the dynamic stiffness reflecting the stiffness and inertia of the surrounding soil. The imaginary component ωC is the product of the circular frequency ω multiplied by a dashpot coefficient C which reflects the material damping and the radiation of energy in the soil-foundation system. The dynamic stiffness is estimated as the product of the static stiffness, K, times the frequency-dependent dynamic stiffness coefficient, k:

$$\overline{K}_i(\omega) = K_i \cdot k_i(\omega) \quad \text{with } i = z, y, x, rx, ry \tag{3}$$

The static stiffness is computed based on the formulas proposed by Gazetas (1991). The spring–dashpot systems have constant properties which are calibrated to the mean frequency of the accelerograms, f_m (Rathje et al. 1998). For the case of the multi-support excitation the spring–dashpots systems are calibrated to the average of the mean frequencies of the accelerograms applied at the four horizontally constrained supports (i.e. the abutments and the pylons).

The complete set of bridges have been analysed by means of the direct response history analysis, assuming that the constituent materials behave in a linear elastic manner during the seismic excitation; an assumption based on the fact that the significance of cable-stayed bridges dictates that they remain elastic even under very strong earthquakes. The

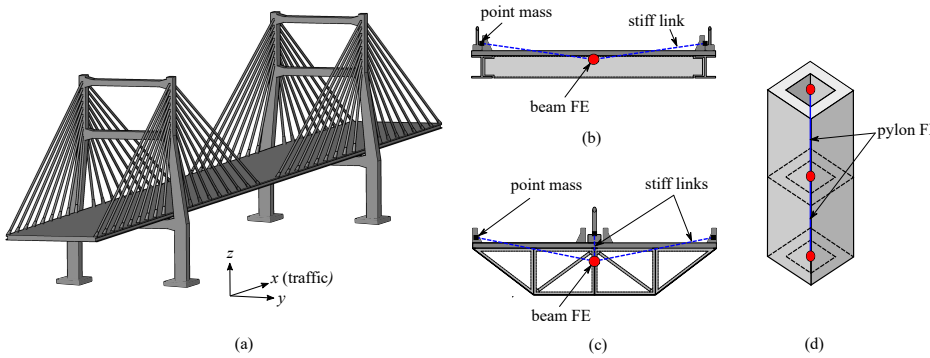

Figure 3. (a) Complete 3D model of the H-LCP model with $L_P = 200$ m, (b) FE model of the LCP deck, (c) FE model of the CCP deck and (d) FE model of the pylon.

time-step in the analysis has been assumed $\Delta t = 0.01$ seconds coinciding with the time-step of the accelerograms, as will be discussed in the following section. The materials (steel and concrete) that have been used in the cable-stayed bridges are described through their constitutive models (Eurocode 2; Part 1.1; Eurocode 3; Part 1.1; Eurocode 3; Part 1.11; Eurocode 8; Part 2). The concrete in the pylons is C40 concrete with Young's modulus $E_c = 35$ GPa and density $\rho_c = 2500$ kg/m^3. The structural steel in the deck is B500C grade with $E_s = 210$ GPa and $\rho_s = 7850$ kg/m^3, while for the prestressing steel in the cables the Young's modulus is $E_p = 190$ GPa. The structural damping is defined by means of the frequency-dependent Rayleigh's distribution. The maximum damping ratio is taken equal to 2% accounting for the low structural dissipation that characterises the elastic response of cable-stayed bridges (Kawashima et al. 1993) and it is independent of the material (concrete or steel). The range of important frequencies for the structural response of the bridges, and consequently the range of modes which are assigned a lower damping than 2%, is defined at the lower bound by the fundamental frequency (f_1) of the bridges. f_1 is equal to 0.50, 0.35 and 0.20 Hz for the 200, 400 and 600-m span bridges, respectively, and it is almost insensitive to the pylon shape and to the type of cable system. The upper bound of the important frequency range is set as 20 Hz in all cases (Camara 2011). For the definition of the variable damping ratio the stiffness-proportional, α_R, and mass proportional, β_R, factors are equal to 0.12 and 0.0031, respectively suggesting that the stiffness-proportional part of the variable damping is more important the mass-proportional one. Consequently, the damping ratio varies between $\xi_{\min} = 0.6\%$ and $\xi_{\max} = 2\%$.

The finite element analysis software Abaqus has been used to model the bridges and to conduct the complete sets of dynamic analyses by means of the implicit HHT algorithm (Hilber et al. 1977). Figure 3 shows that the decks of the LCP and CCP models are discretised with linear interpolation, shear-flexible beam-type elements that pass through the centre of gravity of the sections and account for the structural (i.e. reinforced concrete slab, longitudinal and transverse steel girders and steel diaphragms) and nonstructural

(i.e. deck asphalt) masses, as shown in Figs. 3(b) and 3(c). Lump mass elements located at both cable ends represent the anchorage masses which, at the deck end of each cable, also include the parapets on the deck. The pylons are also modelled with beam-type elements through the centre of gravity of their sections (see Fig. 3(d)). The cables are modelled with 3D trusses which use linear interpolation of the axial displacements. A sensitivity analysis conducted by Efthymiou and Camara (2015) compared the seismic responses of pylons when the discretisation of each cable is done with multiple elements (multiple-element-cable-system; MECS) or with single (single-element-cable-system; SECS) truss elements. Even though the coupled flexure of the cables and the deck was clear in the MECS model, this interaction did not significantly change the first transverse vibration period, T_1. The sensitivity analysis also showed that the peak transverse response, obtained for different main span lengths with the two cable modelling techniques is larger in the SECS model than in the MECS model (up to 40% in the models with $L_P = 400$ m for which modal couplings were observed to be more significant in the studied bridges). The result was found to be in agreement with Caetano et al. (2000) and therefore, SECS models have been considered since the results fall on the safe side and the purpose of the paper is to compare the responses from the synchronous motion of the supports and from the SVGM, where the same assumptions have been made. The geometric nonlinearities arising from the large deformations, a characteristic of cable-stayed bridges (Abdel-Ghaffar and Nazmy 1991), have been accounted for in the analysis.

Seismic Action

When it comes to the consideration of earthquake time-histories the choice between natural or artificial accelerograms needs to be carefully made. Ideally, the study of the SVGM should be accomplished by selecting recorded seismic signals from strong motion arrays provided that the distance between supports matches the distance between stations in the array and that the site characteristics of both regions are similar (Abdel-Ghaffar and Rubin 1983). Another ideal option is to obtain the seismic records from accelerometer arrays that are permanently installed on long and multiply-supported structures(Sextos et al. 2014).

Natural records represent the actual parameters of the ground motion and they are realistically nonstationary both in the time and frequency domains. However, it is not always possible to find records that are compatible with the design spectra in different directions (particularly from the same event), leading either to the scaling of the actual records or to the employment of records that have been recorded in regions with very different soil conditions, source-to-site distances or rupture mechanisms compared to those dictated by the seismic hazard in the site of the structure under consideration. Moreover, scaling of natural records is often required so that their spectral amplitudes match those of the target spectrum. On the other hand, there exist analytical models in order to generate artificial acceleration time-histories which are based on stochastic processes and they represent an adequate and widely accepted approach. Several models have been developed to represent the nonstationarity, the strong motion window of the

signal and its frequency content. Artificial accelerograms also allow to represent the SVGM in the time and the frequency domains directly.

This study aims to assess the effect of the SVGM in cable-stayed bridges and not to examine the seismic response of a particular structure at a particular site. This limits the applicability of natural records, which are strongly influenced by the site in which they were recorded and the magnitude of the event, among other seismological aspects. In addition, there are not sufficient unscaled natural records that can match the proposed design spectra in the range of important vibration periods for the short, intermediate and long-span bridges considered in this paper. A more abstract definition of the seismic action is needed in order to focus on the effect of the SVGM. For this work artificial sets of accelerograms have been generated based on the Eurocode 8; Part 1 elastic response spectrum with 2% damping for ground category D. Although cable-stayed bridges are usually landmark structures for which a specific analysis of the local seismic hazard is conducted, no attempt has been made to relate the proposed design spectrum to any particular location in order to keep the implications of the results general. With this consideration, the study aims at focusing on the influence of different design parameters (e.g. the pylon shape, the pylon–cable system configuration or the length of the bridge) on the SVGM response. For the generation of spectrum-compatible acceleration histories that can be modulated both in time and frequency and that can account for the loss of coherency and time delay of the ground motions due to the SVGM , the iterative methodology proposed by Deodatis (1996) has been adopted. Based on preceding work from Hao et al. (1989) and Abrahamson (1993), Deodatis (1996) proposed an iterative scheme. By initially introducing $S_{jj}(\omega)$ as constant noise for the whole frequency range, stationary histories are generated based on Eq. (4) when four supports are considered:

$$f^{(j)}(t) = 2\sum_{m=1}^{4}\sum_{l=1}^{N}|H_{jm}(\omega_l,t)|\sqrt{\Delta\omega}\cos\left(\omega_l t-\theta_{jm}(\omega_l,t)+\Phi_{ml}\right), \quad j=1,2,3,4 \tag{4}$$

where j represents the support of interest and m the total number of supports between which the stochastic process is established (i.e the first abutment, where $m = 1$, the first pylon, $m = 2$, the second pylon, $m = 3$ and the second abutment, $m = 4$), $\omega_l = l\Delta\omega$ (with l = 1, 2, . . . , N) is the discrete frequency, $\Delta\omega = \omega_u/N$ is the frequency step, ω_u is the cut-off frequency beyond which the cross spectral density matrix has practically no effect on the simulations, Φ_{ml} are independent random phase angles uniformly distributed over the range [0, 2π). Then the RS obtained at the end of the i^{th} iteration from the generated acceleration history at support j, $\text{RS}_j^{(i)}$, is compared to the target $\text{RS}_j^{\text{target}}(\omega)$ and until acceptable convergence is reached the process is repeated with an updated S_{jj} as follows:

$$S_{jj}^{(i+1)}(\omega) = \left[\frac{\text{RS}_j^{\text{target}}(\omega)}{\text{RS}_j^{(i)}(\omega)}\right]^2 S_{jj}^{(i)}(\omega) \tag{5}$$

where: $S_{jj}^{(i+1)}$ is the resulting PSD at station j for the next iteration..

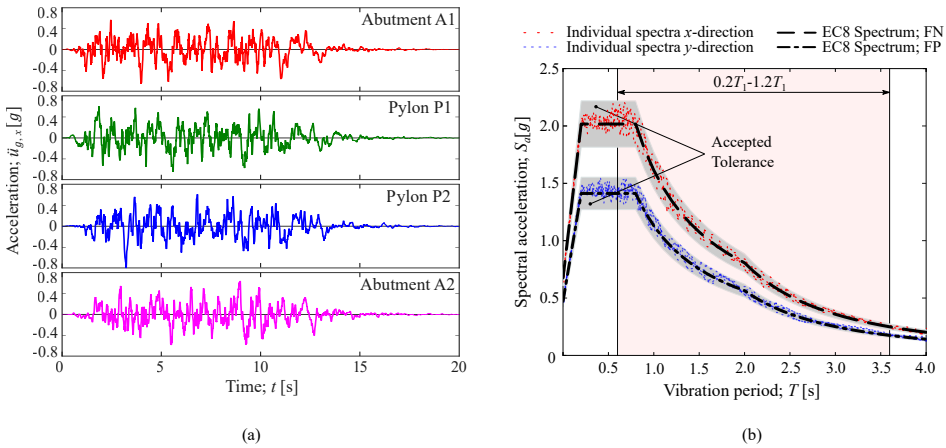

Figure 4. (a) Sample set of accelerograms corresponding to the FN earthquake component, (b) average of the response spectra at the four supports of the bridge. The target spectra are also included. L_P = 400 m, c =1000 m/s.

To account for the loss of coherency among the ground motions at the different supports of the bridges the coherency model of Harichandran and Vanmarcke (1986) has been adopted. This model considers incoherent seismic waves in low frequencies that are important to the seismic response of cable-stayed bridges and is the most appropriate for this work following the findings of Efthymiou and Camara (2017) who examined various empirical and semi-empirical coherency models.

Apart from the loss of coherency, this study also accounts for the temporal variability of the ground motion by means of the delay between the arrival times of the seismic waves at neighbouring supports, which can reach several seconds in long structures such as cable-stayed bridges. The reference support is the first abutment (A1) and then the ground motion propagates parallel to the deck with velocity of propagation $c = 1000$ m/s. The delay between the two pylons reaches 0.2, 0.4 and 0.6 s in the $L_P = 200$-, 400-m and 600-m bridges, respectively. Accordingly, the delay between the end supports (abutments) reaches 0.36, 0.72 and 1.08 s in the $L_P = 200$-, 400-m and 600-m bridges, respectively. The complete generation scheme is detailed in Efthymiou (2019).

The effect of the SVGM on the seismic response of the cable-stayed bridges is highlighted by comparing the response quantity of interest from the SVGM to the respective quantity from the identical support motion i.e. when considering infinite velocity of the seismic waves. This case is referred to as the synchronous motion scenario (SYNC), in which the reference action at abutment A1 is applied to the four supports of the cable-stayed bridges simultaneously.

Seven sets of spectrum-compatible acceleration histories have been generated parallel to the two horizontal components of the seismic action, namely fault-parallel (FP) and fault-normal (FN), the latter coinciding with the direction of wave propagation. Artificial accelerograms are not associated to principal components in their generation process,

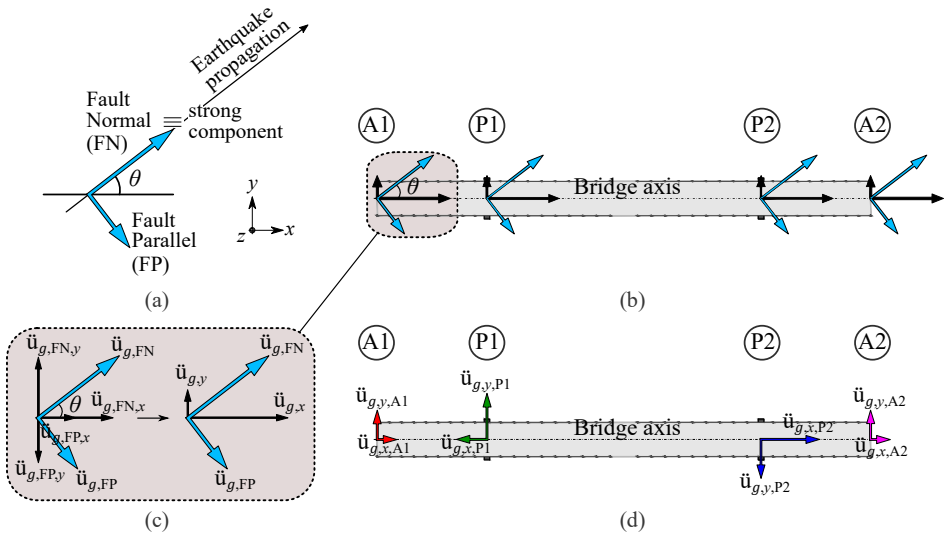

Figure 5. Incidence angle of the seismic waves with respect to the axis of the bridge; (a) principal components of the earthquake, (b) incidence angle θ of the seismic waves and corresponding projected earthquake components (black lines) in the case of synchronous motion of the supports and (c) detailed projection of the principal earthquake components to the local x and y axes of the bridge (*following from (b)*), (d) projected earthquakes $\ddot{u}_{g,\,i,\,j}$, with $i = x$, y and $j =$ A1, P1, P2, A2 at time instance t from the start of the earthquake and for a given coherency γ.

hence an intensity ratio between the major and minor earthquake components has been adopted to account for the observed differences in the propagation of the waves in the directions perpendicular and parallel with respect to the fault. For the generation of the accelerograms corresponding to the FP component, the target spectrum is reduced to 70% to account for the principal components of the earthquake (Lopez et al. 2006). The coherency is assumed independent of the direction of propagation, allowing for the same loss of coherency model to be used for the generation of signals in the FN and FP directions (Hao 1989; Sextos et al. 2003). The resulting accelerograms are considered acceptable when the obtained response spectrum of each signal falls within the range 90%–110% of the target spectrum in the range of important periods of the bridges: $[0.2T_1, 1.2T_1]$, T_1 being the fundamental vibration period of the structure in each case (Camara 2011). Considering the seven different structural typologies, T_1 is 2.0, 2.87 and 5.09 s on average when $L_P = 200$, 400 and 600 m, respectively. The generated accelerogram sets have been baseline-corrected. An indicative set of accelerograms generated for the supports of the 400-m main span bridge is presented in Fig. 4(a), where the time delay and the loss of coherency between supports can be appreciated. Figure 4(b) shows a good match between the FN and FP target spectra and those of the resulting accelerograms.

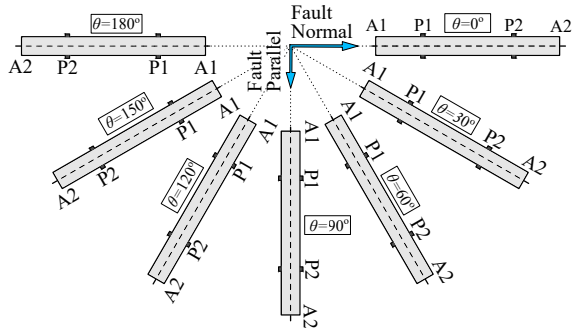

Figure 6. Rotation of the bridge to examine the effect of the angle of incidence of the seismic waves in the range of 0° to 180° with 30° increments.

In order to explore the effect of the angle of incidence of the seismic waves, the bridges are rotated in the range of 0° to 180° with increments of 30°. Figure 5 shows that the axis of the bridge forms an angle θ with the FN component of the earthquake. When $\theta = 0°$ the FN component coincides with the bridge axis and when $\theta = 90°$ the bridge is rotated clockwise so that the FP component is aligned with the bridge axis. In the intermediate angles of incidence, the accelerograms are projected to the local x (bridge axis) and y axes of the bridge by means of the rotation matrix of Eq. (6):

$$\begin{pmatrix} \ddot{u}_{g,x} \\ \ddot{u}_{g,y} \end{pmatrix} = \begin{pmatrix} \cos\theta & \sin\theta \\ \sin\theta & -\cos\theta \end{pmatrix} \begin{pmatrix} \ddot{u}_{g,\mathrm{FN}} \\ \ddot{u}_{g,\mathrm{FP}} \end{pmatrix} \tag{6}$$

The different orientations of the cable-stayed bridges are shown in Fig. 6.

Multi-Angle Response

This section discusses the influence of the orientation of the bridge with respect to the earthquake propagation by examining the arithmetic mean (μ) of the peak seismic forces in the pylons under different values of θ. The results are presented in Fig. 7 in the form of polar plots for the H-LCP model with $L_P = 400$ m. These are created for the mean peak seismic axial load (N), longitudinal shear force (V_x) and transverse shear force (V_y) at the base and at the deck level of the pylon. The seismic response strongly depends on the value of θ. This is mainly due to the larger spectral acceleration in the direction normal to the fault ($S_{a,\mathrm{FP}} = 70\%\, S_{a,\mathrm{FN}}$). The longitudinal shear force in the pylon (middle column in Fig. 7) is maximised when the FN earthquake component is parallel ($\theta = 0°$ or 180°) to the deck. Accordingly, V_y (right column in Fig. 7) is maximised when the FN component is perpendicular ($\theta = 90°$) to the deck. The axial load, N, is also maximum at $\theta = 90°$ suggesting that the axial response of the pylon is dominated by the transverse flexure of the bridge. 'H'-shaped pylons have two legs that resist the lateral movement which induces tension in one leg and compression in the other, explaining why N and V_y are maximised in the same orientation of the bridge (Efthymiou 2019). The minimum

seismic response is usually obtained by rotating the earthquake by 90° from the angle in which the response is maximum, so that the FP component is aligned with the direction of the response under consideration. The ratio between the minimum and the maximum responses for different bridge orientations is approximately 0.7, which coincides with the ratio between the spectral accelerations of FP and the FN target spectra.

The SVGM has a more pronounced effect on the longitudinal than on the transverse response at the base and the deck level of the pylon, which generally falls within the limits of the dispersion of the results obtained from the SYNC motion in the latter direction of the seismic response. In the majority of the bridge orientations the SVGM reduces V_x compared to the SYNC motion and it increases V_y at the pylon base.

The difference in the values of N and V_y when $\theta = 30°$ and $\theta = 120°$ that is observed in the response from the SVGM is due to the time-lag and to the fact that depending on the value of θ, the pylon under consideration receives first or second the ground motion. For example when $\theta = 30°$ pylon P2 is the second pylon to be reached by the seismic waves, but when $\theta = 120°$ P2 receives the earthquake first, as detailed in Fig. 6. When the ground motion at the two pylons is not identical (i.e. when the SVGM is considered) it can lead to differences in the response of the pylon for different values of θ.

In order to quantify the effect of the SVGM on the seismic behaviour of the bridges, the response ratio ρ_j is calculated as;

$$\rho_j = \frac{R_{\text{SVGM},j}}{R_{\text{SYNC},j}} \tag{7}$$

where $R_{i,j}$ with $i =$ SVGM, SYNC is the arithmetic mean (from the seven sets of accelerograms) of the peak response quantity under consideration: $j = V_x$,V_y. When $\rho_j > 1$, the SVGM is considered important because it increases the seismic response compared to the SYNC motion. Figure 8 presents this ratio in polar form obtained from the longitudinal and the transverse shear forces at the base of the pylon. This represents a critical region in the pylon in terms of the peak longitudinal seismic response and of the

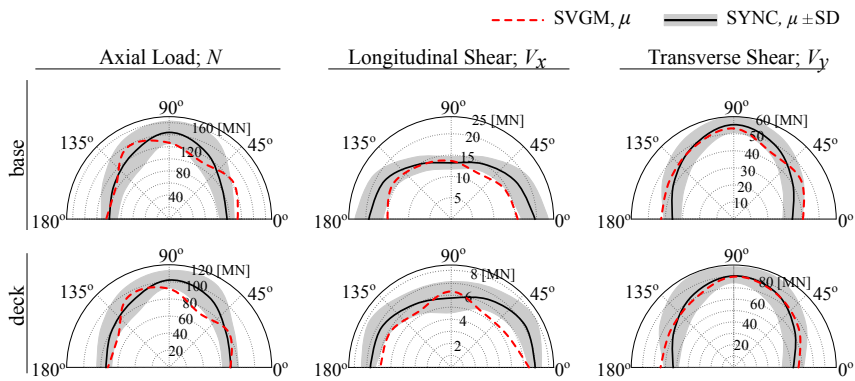

Figure 7. Peak seismic response at critical sections of the pylon for different incidence angles (θ). H-LCP model, $L_P = 400$ m.

maximum effect of the SVGM in the transverse response. The ratio is presented for the H-LCP model with $L_P = 400$ m.

The results show that the transverse response ratio, ρ_{V_y}, is larger than the longitudinal ratio, ρ_{V_x}, confirming that the effect of the SVGM at the base is more important in the transverse direction. It is observed that V_x is reduced at the base of the pylon (i.e. $\rho_{V_x} < 1$) when the bridge is subjected to non-uniform motions for all incidence angles except for $\theta = 90°$, where $\rho_{V_x} \simeq 1$. Therefore, it can be stated that the SVGM is not detrimental for the seismic response at this region of the pylon from the point of view of the longitudinal seismic forces. On the other hand, the base of the pylon is more vulnerable in the transverse than the longitudinal direction from the SVGM, with ρ_{V_y} taking values of up to 1.2 when the FN component is parallel to the bridge ($\theta = 0°$ and 180°). It is interesting to note the shape of the polar plots of Fig. 8 compared to the respective polar plots for the longitudinal and the transverse seismic shear forces of Fig. 7. The maximum effect of the SVGM (i.e. $\rho_{V_x,\text{max}}$ and $\rho_{V_y,\text{max}}$) is obtained in the direction where the response (i.e. V_x and V_y) is maximised. This finding proves that the critical orientations of the bridge when the maximum seismic response in terms of V_x or V_y is obtained do not coincide with the orientations for which the effect of the SVGM is more significant. However, it is also found that in the case of the intermediate-span bridge ($L_P = 400$ m) the principal orientations of the bridge — the ones wherein the FN (strong) or the FP (weak) components are aligned with the deck (i.e. $\theta = 0°$, 90° and 180°) — are the most important ones for the SYNC and the SVGM responses.

Influence of the Main Span Length

The discussion will focus now on the seismic response of the pylons in bridges with different spans under the SVGM and the SYNC ground motions when the FN component is aligned with the deck: $\theta = 0°$. Figure 9 presents the longitudinal (top row) and the transverse (bottom row) shear forces in the pylon of the H-LCP bridge models with $L_P =$ 200, 400 and 600 m (i.e. $H_{tot} = 62.5$, 125 and 187.5 m, respectively). The results show that the SVGM can reduce or increase the peak SYNC response, depending on the part of the pylon under consideration, on the length of the bridge and on the direction of the response.

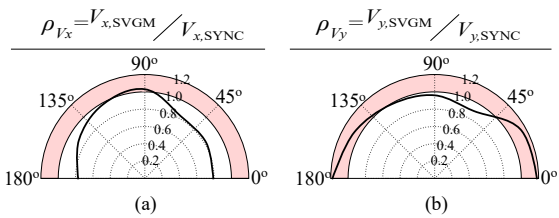

Figure 8. Polar ratio ρ of the (a) longitudinal shear force (V_x) and (b) transverse shear force (V_y) at the base of the pylon for different incidence angles (θ). $L_P = 400$ m. The coloured band denotes $\rho > 1.0$, for which the SVGM increases the seismic response.

Figure 9 distinguishes three regions of the pylon on which the effect of the SVGM is significant; the top part of the pylon which holds the anchorage system, the inclined part of the legs between the intermediate and the lower transverse struts, and the region below the transverse strut down to the base. In the middle of the inclined legs of the pylon in the $L_P = 200$-m bridge the peak seismic V_x is reduced by approximately 20% when the SVGM is considered (Fig. 9(a)), but V_y in the same region is increased by 30%. Considering the transverse response, the effect of the SVGM varies depending on the region of the pylon in which it is examined. Figure 9(b) shows that in the $L_P = 400$-m bridge the SVGM reduces V_y by 25% at the level of the bottom anchorage compared to the SYNC motion, but increases it by 18% at the base of the pylon, highlighting that the effect of the SVGM depends on the region of the pylon and the response quantity of interest.

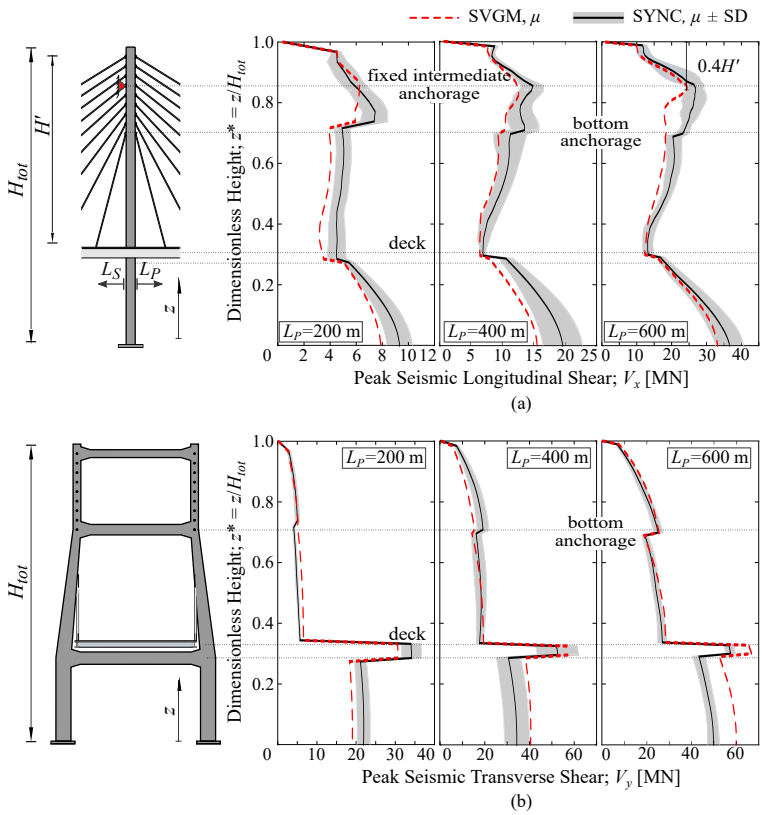

Figure 9. Effect of the SVGM for different main span lengths (L_P) on the peak seismic response of pylon P2: (a) longitudinal shear force V_x, (b) transverse shear force V_y. H-LCP model; $\theta = 0^\circ$.

In the longitudinal direction the effect of the SVGM generally reduces the seismic response of the pylon compared to the SYNC motion, as shown in Fig. 9(a), regardless of L_P. The influence of the SVGM is not significant in the transverse response of the pylons above the deck level (Fig. 9(b)) because in this part of the pylons the cable system hardly restrains their lateral movement. However, the effect of the SVGM in the transverse direction can be appreciable at the connection between the deck and the pylon down to the base where the increment of V_y is observed. This results from the constraint between the deck and the pylon through the rigid transverse connection between them, and also from the larger sections of the legs at the base compared to the inclined and top parts of the legs (Camara et al. 2014). Due to the lateral restraint of the pylon movement provided by the deck, the deck–pylon reaction increases up to 20% in the 600-m span bridge under the SVGM, which is responsible for the larger seismic forces that are observed below the lower transverse strut of the 'H'-shaped pylon. The increasing influence of the SVGM is noticed in the transverse response of the $L_P = 200$- and 400-m bridges and it is attributed to the increased influence of the vibration modes that couple the transverse flexure of the pylons and the deck, which are of increasing order as the main span increases (Camara and Efthymiou 2016).

The increase in the height of the pylons that results from the increase in the main span length $\left(H = {}^{L_P}/_{4.8}\right)$ is not directly associated with the effect of the SVGM, as the current codes of practice imply by associating the effect with the SVGM to the length of the bridge (Eurocode 8; Part 1). Specifically, at the level of the bottom anchorage the transverse shear force from the SVGM is increased by 25% compared to the SYNC motion in 200-m span bridge, but it is reduced by 25% in the 400-m span bridge and it is similar for both SVGM and SYNC in the 600-m span bridge. On the other hand, the effect of the SVGM is larger at the base of the longest bridge compared to its intermediate-span and shortest counterparts and this is due to the largest sections of the pylons with increasing height, making them stiffer and hence, more susceptible to the SVGM.

Influence of the Pylon Shape

This section explores how the geometry of the pylons affects their seismic response when subjected to non-uniform ground motions. Given that the differences among the pylon geometries are mostly relevant in the direction perpendicular to the deck and that the SVGM is more pronounced in this direction (Figs. 8 and 9(a)), the transverse magnitude of the SVGM (ρ_{V_y}) is considered as the basis for the discussion in this section.

Figure 10 shows the transverse response ratio, ρ_{V_y}, along the height of the pylons with different shapes. The effect of the SVGM on the seismic response varies with the pylon shape and with the region of the pylon that is examined. However, the SVGM consistently increases the transverse response of the pylons below the deck level down to their base regardless of the pylon shape, with ρ_{V_y} ranging from 1.1 to 1.5 due to the transverse force exerted by the deck. The exception is the lower part of the pylon in the Y-LCP model in which the SVGM and the SYNC motion result in the same transverse shear force ($\rho_{V_y} \simeq 1$). Interestingly, the minimum value of ρ_{V_y} is observed for the Y-LCP model, whereas the maximum value of ρ_{V_y} occurs for the YD-LCP model (i.e. inverted 'Y'-shaped pylon

with a lower diamond) in which the lateral legs of the pylons are connected to a single vertical pier below the transverse strut. This is attributed to the change in the inclination of the individual legs below the deck in the YD-LCP bridge (Fig. 1(d), (e)).

At the intermediate part of the legs, between the deck level and the anchorage of the bottom cable, only the pylons with lower diamonds have increased V_y from the SVGM compared to the SYNC motion. These pylons are of inverted 'Y' and 'A' shapes (i.e. YD-CCP, YD-LCP and AD-LCP models) and they have in common the high inclination of their intermediate legs, which is reversed below the deck until they are connected to the common vertical member at the bottom (Fig. 1(c), (e) and (g)). On the other hand, the intermediate part of the Y-CCP, Y-LCP and A-LCP models, whose individual legs have constant inclination along their height, is not vulnerable to the SVGM (i.e. $\rho_{V_x} < 1$ between the bottom anchorage and the deck).

Generally, the pylons with two individual legs throughout their height are better candidates to resist the SVGM compared to the ones with lower diamonds. The SVGM increases the transverse displacement at the top of the YD-LCP pylon by 45% from the SYNC motion, whereas in the Y-LCP model the transverse displacement from the SVGM is 5% smaller than that from the SYNC motion. Similarly, in the 'A'-shaped pylons with and without lower diamonds there is an increase of 37% and 6%, respectively in the transverse displacement at the top when the pylons oscillate out-of phase compared to the SYNC motion. Figure 11 presents the variation in the required longitudinal reinforcement, A_s, from the SVGM compared to the SYNC motion at the base of the different pylons by means of the ratio ρ_{A_s}. The large transverse displacements of the pylons under the SVGM are also reflected in the required longitudinal reinforcement at the base of the pylons of the YD-LCP and AD-LCP bridges with $L_P = 400$ m, which is increased by 69% and 46%, respectively from the required reinforcement when SYNC motion of the supports is considered, as shown in Fig. 11. On the other hand, a smaller increase is observed at

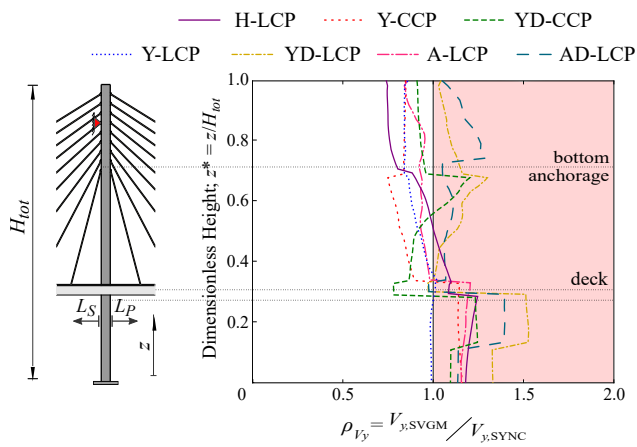

Figure 10. Transverse response ratio ρ_{V_y} along the height the of pylon. $L_P = 400$ m, $\theta = 0^\circ$. The coloured band denotes $\rho_{V_y} > 1.0$, for which the SVGM increases the seismic response.

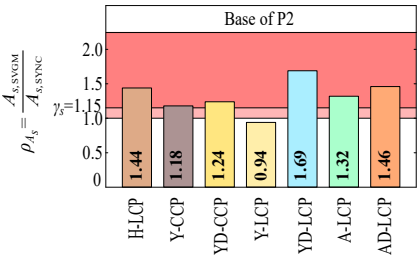

Figure 11. Variations in the required longitudinal reinforcement, A_s, from the SVGM compared to the SYNC motion at the base of the seven pylon configurations when $L_P = 400$ m by means of ratio ρ_{A_s}. The light and dark coloured bands denote slight and large increase in the reinforcement from the SVGM compared to the SYNC motion, respectively.

the base of the same pylons without lower diamonds where the required reinforcement resulting from the SVGM is 6% less and 32% more in the Y-LCP and A-LCP models, respectively compared to the SYNC motion. However, in all pylon configurations, with the exception of the Y-LCP pylon, the base section is significantly affected by the SVGM resulting in greater reinforcement ratios than the SYNC motion. These cannot be accommodated by the steel safety factor $\gamma_s = 1.15$, as defined in Eurocode 2; Part 1.1 and therefore it is verified that the SVGM needs to be considered in the design of cable-stayed bridges particularly with pylons that have lower diamonds.

Effect of the Cable System

The peak seismic response of the $L_P = 400$-m bridge with inverted 'Y'-shaped pylons is compared in Fig. 12 for central and lateral cable systems (CCP and LCP, respectively). It should be noted that due to the influence of the cable arrangement on the cross-section of the deck, the latter is 1.25–1.3% stiffer and 12.5% heavier in the bridge with one CCP and 400 m main span, in comparison to the homologue LCP structure. Figure 2(d) shows the differences between the decks of the CCP and LCP bridge. However, Fig. 10 shows that the changes in the stiffness and the mass of the decks between the two deck–cable system

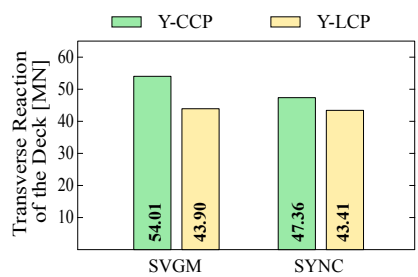

Figure 12. Peak transverse seismic reaction of the deck to the pylons legs in the Y-CCP and Y-LCP models for the SVGM and for the SYNC motion case. $L_P = 400$ m, $\theta = 0^\circ$.

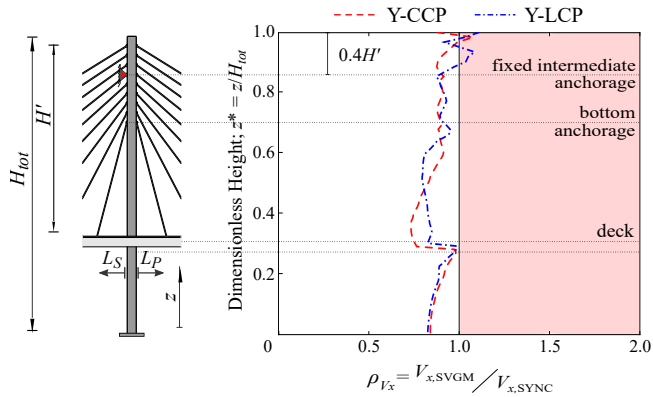

Figure 13. Longitudinal response ratio ρ_{V_x} in the pylon of the Y-CCP and Y-LCP models. $L_P = 400$ m, $\theta = 0°$. The coloured band denotes $\rho_{V_x} > 1.0$, for which the SVGM increases the seismic response.

configurations, cannot explain alone the increased effect of the SVGM in the lower part of the pylon in the Y-CCP model, where $\rho_{V_y} = 1.17$ and 1.0 for the pylons of the Y-CCP and Y-LCP models, respectively. On the other hand, the effect of the cable system on V_y is minimised at the anchorage area in the pylon, where ρ_{V_y} is identical between the two models. Figure 12 shows that when SYNC motion is considered the Y-CCP bridge with $L_P = 400$ m maximises the transverse deck-pylon reaction, which is 10% larger than the one in the Y-LCP bridge and it is mainly attributed to the 12.5% increment in the weight of the deck. This difference is increased to 24% when the pylons move asynchronously in the transverse direction under the SVGM.

In the longitudinal direction (ρ_{V_x}) in which the SVGM reduces the seismic response along the pylons of the Y-CCP and the Y-LCP models when $\theta = 0°$ (i.e. FN // deck). The exception is at the top part of the cable system above the intermediate anchorage in the CCP and LCP models, as can be seen in Fig. 13, where the SVGM slightly increases V_x compared to the response from the SYNC motion by 10% ($\rho_{V_x} = 1.1$), concluding that the effect of the cable system in the response from the SVGM is more significant in the transverse direction, i.e. $\rho_{V_y} > \rho_{V_x}$. This is explained by the different configuration of the cable anchorages along the deck in CCP and LCP bridges. When the bridge has a single CCP the cables are perpendicular to the deck and the transverse seismic loads coming from the girder are concentrated to the deck-pylon connection. However, in LCP bridges the two cable planes are anchored at the edges of the deck and an additional path is provided through the inclined cable system to transmit the transverse deck loads to the pylons.

Modal Contribution to the Seismic Response

In this section the effect of the multi-support excitation on the frequency content of the pylons' vibration is explored. In order to examine the participation of different modes to the seismic response, the time-histories of the axial load and of the longitudinal and the transverse shear forces at the base of the pylons during the earthquakes (removing the contribution of the permanent loads) have been studied. Figure 14 compares the response time-histories of the axial force at the base of pylon P2 (position S1) from the SVGM and from the SYNC motion in the bridges with a central cable system with or without the lower diamond configuration (i.e. Y-CCP and YD-CCP).

The difference in the response of different pylons under the SVGM can be explained by the changes in the contribution of certain vibration modes. The relatively close spacing between consecutive peaks in the response time-history of the axial load from the SVGM at the base of the pylon with a lower diamond in Fig. 14(b) indicates that the response is dominated by higher-order vibration modes compared to those contributing to the axial response of the pylon without a lower diamond. According to previous studies on the seismic response of cable-stayed bridges under SYNC motion, the mode that governs the axial load in the pylon involves the vertical deformation of the lateral legs, which are especially stiff in the lower diamond pylons due to the dimensions of the vertical pier below the deck (Camara 2011). However, when the ground motion is asynchronous the axial response in the pylons with lower diamonds is dominated by a low-order vibration mode, as shown in Fig. 14(b). This is observed for all the records but only in bridges with lower diamonds. The effect is further explored in Fig. 15, which presents the frequency content of the response time-history included in Fig. 14 for earthquake record #1 by means of the fast Fourier transform (FFT). The FFT shows that in the 400-m span YD-CCP bridge under the SVGM the contribution to the axial response of the fundamental mode (f_1), which involves the transverse flexure of the deck, increases significantly and becomes dominant: $f_{1,N} = f_1 = 0.35$ Hz in Fig. 15(b) (where $f_{1,j}$ represents the dominant mode in the response j, with $j = N, V_x, V_y$). This mode is responsible for the low-frequency oscillation observed in the time-history illustrated in Fig. 14(b). However, the frequency content of the axial response of the bridge with inverted 'Y'-shaped pylons without lower diamonds from the SYNC motion and the SVGM is dominated by the higher transverse mode #11 of the pylons, as shown in Fig. 15(a). This happens because inverted 'Y'-shaped pylons without lower diamonds are very stiff in the transverse direction due to the constraint provided by the connection of the two lateral legs above the deck and the large inclination of their legs (Camara and Efthymiou 2016). The main difference with the YD-CCP model is that the pylons with lower diamonds have certain rotation capacity at the connection between the lateral legs and the vertical pier below the deck, which helps to accommodate the differential pylon movements in the transverse direction. This effect ultimately reduces (by up to 60%) the peak axial load in the pylon of the YD-CCP bridge in comparison to that of the Y-CCP bridge when the SVGM is considered.

By exploring the shapes of important vibration modes included in Fig. 15 it is observed that the axial response of both bridges under SYNC motion is significantly affected by longitudinal and transverse modes in which the movement of the pylons occurs in the same direction (longitudinal or transverse). This is the case of Modes #11 and #27 in the Y-CCP bridge and of modes #1, #4 and #40 in the YD-CCP model. However under

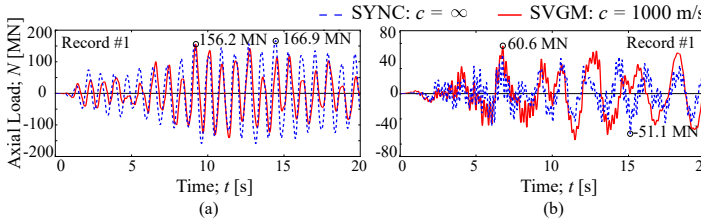

Figure 14. Response time-history of the seismic axial force (N) at the base of pylon P2 in models: (a) Y-CCP, (b) YD-CCP. Earthquake record #1, $\theta = 0°$, $L_P = 400$ m. The peak responses are annotated.

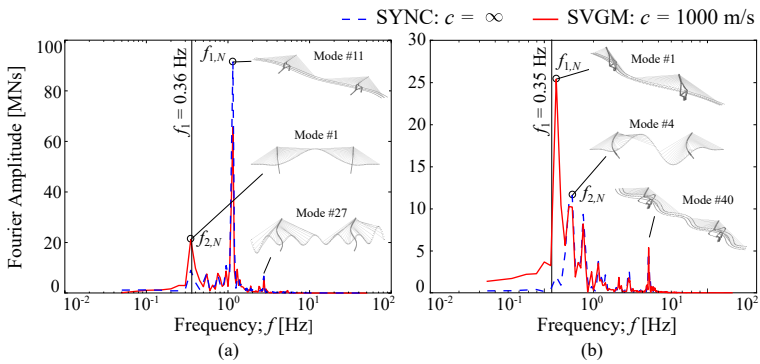

Figure 15. Frequency content of the seismic axial load (N) at the base of pylon P2 in models: (a) Y-CCP, (b) YD-CCP. Record #1, $\theta = 0°$, $L_P = 400$ m.

the SVGM, modes with opposite movement of the pylons, and usually lower frequencies, gain importance. This is the case of mode #1 (fundamental vertical mode with opposite longitudinal movement of the pylons) in the YD-CCP bridge. This result confirms that the SYNC motion excites symmetric modes in symmetric cable-stayed bridges, whereas the SVGM also excites antisymmetric modes, which was first pointed out by Zerva Zerva (1990) in multi-span beams.

It has been observed here that the axial force in the pylons is affected by the longitudinal and the transverse response of the bridge. The discussion will now focus on the longitudinal and the transverse shear forces at the base of the pylon in order to isolate the response of the bridge in each of the two principal directions. Figure 16 shows the evolution of the longitudinal and the transverse shear forces at the base of pylon P2 during earthquake #1 in the two CCP models. The response time-history suggests that the longitudinal shear force is governed by vibration modes with higher frequencies than the transverse response, which is confirmed in the corresponding frequency content of the response presented in Fig. 17. It is also observed that the shear forces in both directions (and the corresponding bending moments) induced by the SVGM in the pylons are dominated by the same frequencies as the ones observed under the SYNC motion:

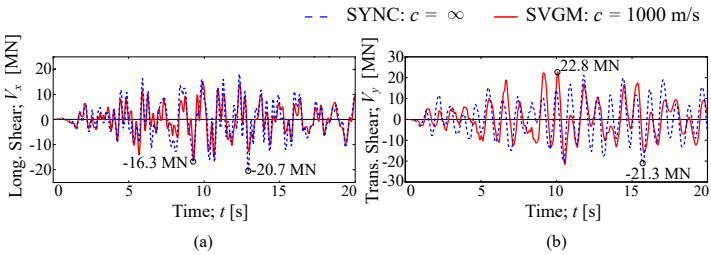

Figure 16. Response time-history of (a) the longitudinal (V_x) and (b) the transverse (V_y) shear forces at the base of pylon P2 in the Y-CCP bridge. Record #1, $\theta = 0°$, $L_P = 400$ m. The peak responses are annotated.

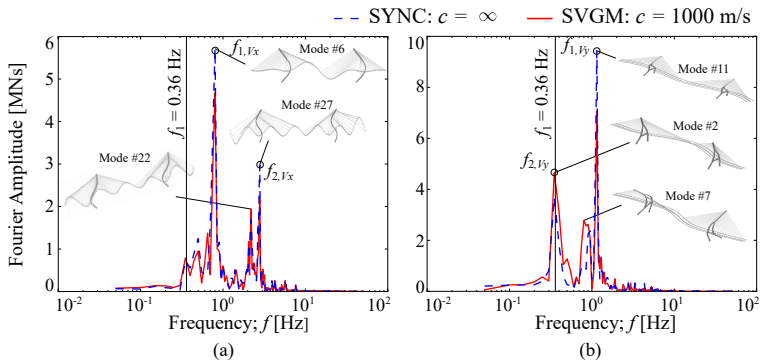

Figure 17. Frequency content of: (a) longitudinal shear force (V_x), (b) transverse shear force (V_y). Results at the base of pylon P2 in the Y-CCP model. Record #1, $\theta = 0°$, $L_P = 400$ m.

$f_{1,V_x} = 0.78$ Hz being the dominant vibration frequency in the longitudinal direction (Fig. 17(a)), and $f_{1,V_y} = 1.14$ Hz for the transverse one (Fig. 17(b)). Nevertheless, the contribution of these frequencies to the total response changes under the SVGM. Figure 17(b) shows that the asynchronous motion of the pylons reduces the presence of the dominant vibration mode in the transverse response of the pylon (f_{1,V_y}). This figure also highlights that the antisymmetric mode #7 ($f_7 = 0.81$ Hz) has a significant contribution to the transverse response of the bridge under the SVGM, as opposed to the SYNC motion in which it is de-amplified. This is explained by the opposite movement of the pylons in mode #7. On the other hand, the longitudinal shear force at the pylon base is smaller under the SVGM because the contribution of the dominant vibration modes #6 ($f_6 = 0.78$ Hz) and #27 ($f_{27} = 2.72$ Hz) is reduced.

Conclusions

This paper has examined the effect of the SVGM on the seismic response of the pylons of cable-stayed bridges. Seven different pylon–cable system configurations and three main span lengths (L_P) of 200, 400 and 600 m have been considered. The earthquake incidence angle with respect to the bridges has been examined, combined with the effect

of the SVGM in terms of the incoherence and wave passage effects. The main conclusions of this study are summarised in the following:

1. The effect of the SVGM varies depending on the response quantity of interest and the region of the pylons in which it is considered. The SVGM generally reduces the longitudinal seismic shear force in the pylon. In the transverse direction, the reaction of the deck to the pylons when the latter oscillate asynchronously can increase considerably their transverse seismic response.
2. The longitudinal response of the pylon is maximised when the fault-normal earthquake component is aligned with the deck, whereas the transverse response maximised if the deck is perpendicular to this component (i.e. fault parallel // deck). However, the maximum effect of the SVGM does not coincide with the directions of the maximum response. The full assessment of the seismic response of a cable-stayed bridge requires several orientations with respect to the earthquake propagation and these should include at least the principal orientations ($\theta = 0^\circ$ and 90°), in which one of the two earthquake components is aligned with the deck, or the range of orientations from 0° to 180° for a more complete assessment.
3. The overall dimensions of the bridge influence the effect of the SVGM on the pylon but increasing the span length is not directly associated with larger effect from the SVGM. The SVGM typically increases the seismic response in the stiffer regions of the pylons which are, in turn, affected by their overall size and by the dimensions of their sections. In longer bridges (400 and 600 m spans) the effect of the SVGM tends to be more pronounced at the bottom part of the pylon, from the deck down to the base. The increasing dimensions of this part of the pylons with increasing height, makes it more vulnerable against the pseudo-static forces introduced by the differential movement of the supports.
4. Bridges with a central cable plane tend to maximise the effect of the SVGM at the lower part of the pylon in the transverse direction, where the pylon shape also plays an important role in the response. Pylons with lower diamonds are more affected by the SVGM, mainly because of the large stiffness of the vertical pier at their base, and also due to the rotation capacity of the connection between this member and the inclined legs of the pylon below the deck, which maximises the transverse displacement of the pylon. On the other hand, the individual legs of the 'H'-shaped pylons or the bridges with inverted 'Y'-shaped pylons and central cable systems with and without lower diamonds are better candidates to accommodate the SVGM above the deck because they are more 'flexible' than the inverted 'Y'-shaped pylons with two cable planes and the 'A'-shaped pylons.
5. There is a close link between the effect of the asynchronous motion on the seismic response and the vibration modes of the structure. Higher-order antisymmetric vibration modes are excited by the SVGM and are de-amplified by the SYNC motion.

References

Abaqus (2018) *ABAQUS 2018. Finite elements analysis program; Providence, RI, Dassault Systèmes Simulia*.

Abdel-Ghaffar A (1991) Cable - stayed bridges under seismic action. In: *Cable - stayed Bridges; Recent Developments and their Future*. Yokohama (Japan): Elsevier Science Ltd., pp. 171–192.

Abdel-Ghaffar A and Khalifa M (1991) Importance of cable vibration in dynamics of cable-stayed bridges. *Journal of Engineering Mechanics* 117: 2571–2589.

Abdel-Ghaffar A and Nazmy A (1991) 3D nonlinear seismic behavior of cable-stayed bridges. *Journal of Structural Engineering* 117: 3456–3476.

Abdel-Ghaffar A and Rubin L (1983) Lateral earthquake response of suspension bridges. *Journal of Structural Engineering* 109: 664–675.

Abrahamson N (1993) Spatial variation of multiple support inputs. In: *1st U.S. Seminar on Seismic Evaluation and Retrofit of Steel Bridges*. University of California at Berkeley (San Fransisco).

Abrahamson N, Schneider J and Stepp J (1991a) Empirical spatial coherency functions for applications to soil-structure interaction analyses. *Earthquake Spectra* 7: 1–27.

Abrahamson N, Schneider J and Stepp J (1991b) Spatial coherency of shear waves from the Lotung Taiwan Large-Scale Seismic Test. *Structural Safety* 10: 145–162.

Allam S and Datta T (2004) Seismic response of a cable-stayed bridge deck under multi-component non-stationary random ground motion. *Earthquake Engineering & Structural Dynamics* 33: 375–393.

Bi K, Hao H and Ren W (2010) Response of a frame structure on a canyon site to spatially varying ground motions. *Structural Engineering and Mechanics* 36: 111–127.

Bolt B, Loh C, Penzien J, Tsai Y and Yeh Y (1982) Preliminary report on the SMART-1 strong motion array in Taiwan. Technical report, Earthquake Engineering Research Center Report No. UCB/EERC-82/13, University of California, Berkeley CA.

Burdette N, Elnashai A, Lupoi A and Sextos A (2006) The effect of asynchronous earthquake motion on complex bridges. Technical report, Mid-America earthquake center, Department of civil engineering, University of Illinois at Urbana-Champaign.

Caetano E, Cunha A and Taylor CA (2000) Investigation of dynamic cable–deck interaction in a physical model of a cable-stayed bridge. Part II: seismic response. *Earthquake engineering & structural dynamics* 29(4): 499–521.

Camara A (2011) *Seismic behaviour of cable-stayed bridges: Design, analysis and seismic devices*. PhD Thesis, Universidad Politécnica de Madrid, Spain.

Camara A, Astiz M and Ye A (2014) Fundamental mode estimation for modern cable-stayed bridges considering the tower flexibility. *Journal of Bridge Engineering* 19.

Camara A and Efthymiou E (2016) Deck-tower interaction in the transverse seismic response of cable-stayed bridges and optimum configurations. *Engineering Structures* 124: 494–506.

Chen MT and Harichandran R (2001) Response of an earth dam to spatially varying earthquake ground motion. *Journal of Engineering Mechanics* 127: 932–939.

Chen W and Duan L (2014) *Bridge engineering handbook. Second edition: Seismic design*. CRC Press.

Deodatis G (1996) Non-stationary stochastic vector processes: seismic ground motion applications. *Probabilistic Engineering Mechanics* 11: 149–168.

Der Kiureghian A (1996) A coherency model for spatially varying ground motions. *Earthquake Engineering & Structural Dynamics* 25: 99–111.

Der Kiureghian A and Neuenhofer A (1992) Response spectrum method for multi support seismic excitations. *Earthquake Engineering & Structural Dynamics* 21: 713–740.

Duan X (2012) Experimental study on seismic performance of cable-stayed bridge tower subjected to longitudinal strong ground motions (in Chinese). *Tongji University, Shanghai* .

Efthymiou E (2019) *The effect of multi-angle spatially variable ground motions on the seismic behaviour of cable-stayed bridges*. PhD Thesis, City, University of London.

Efthymiou E and Camara A (2015) Spatial variability effects of the seismic action in cable-stayed bridges and modelling techniques. In: *IABSE Conference – Structural Engineering: Providing Solutions to Global Challenges*. Geneva (Switzerland).

Efthymiou E and Camara A (2017) Effect of spatial variability of earthquakes on cable-stayed bridges. *Procedia Engineering* 199: 2949–2954.

Efthymiou E and Camara A (2021) Inelastic response of cable-stayed bridges subjected to non-uniform motions. *Bulletin of Earthquake Engineering* 19(6): 2691–2710.

Eurocode 2; Part 1.1 (2004) *Eurocode 2: Design of concrete structures. Part 1.1: General rules and rules for buildings*. EN 1992-1-1:2004.

Eurocode 3; Part 1.1 (2005) *Eurocode 3: Design of steel structures. Part 1.1: General rules and rules for buildings*. EN 1993-1-1:2005.

Eurocode 3; Part 1.11 (2006) *Eurocode 3: Design of steel structures. Part 1.11: Design of structures with tension components*. EN 1993-1-11:2006.

Eurocode 8; Part 1 (2004) *Eurocode 8: Design of structures for earthquake resistance. Part 1: General rules, seismic actions and rules for buildings*. EN 1998-1:2004.

Eurocode 8; Part 2 (2005) *Eurocode 8: Design of structures for earthquake resistance. Part 2: Bridges*. EN 1998-2:2005.

Gazetas G (1991) Formulas and charts for impedances of surface and embedded foundations. *Journal of Geotechnical Engineering* 117(9): 1363–1381.

Gimsing N and Georgakis C (2012) *Cable-supported bridges concept and design. Third edition*. John Wiley & Sons, Ltd.

Hao H (1989) *Effects of spatial variation of ground motions on large multiply-supported structures*, volume 89. Earthquake Engineering Research Center, University of California Berkeley, CA.

Hao H (1997) Pipeline response to random ground motion. *Stability of simple beam subjected to multiple seismic excitations* 123: 739–742.

Hao H, Oliveira C and Penzien J (1989) Multiple-station ground motion processing and simulation based om SMART-1 array data. *Nuclear Engineering and Design* 111: 293–310.

Harichandran R and Vanmarcke E (1986) Stochastic variation of earthquake ground motion in space and time. *Journal of Engineering Mechanics* 112: 154–174.

Hilber H, Hughes T and Taylor R (1977) Improved numerical dissipation for time integration algorithms in structural dymanics. *Earthquake Engineering and Sructural Dynamics* 5: 283–292.

Hindy A and Novak M (1980) Pipeline response to random ground motion. *Journal of the Engineering Mechanics Division* 106: 339–360.

Kawashima K, Unjoh S and Tunomoto M (1993) Estimation of damping ratio of cable-stayed bridges for seismic design. *Journal of Structural Engineering* 119(4): 1015–1031.

Khan R (2012) *Earthquake-Resistant Structures – Design, Assessment and Rehabilitation*, chapter Seismic reliability analysis of cable-stayed bridges against first passage failure. INTECH Open Access Publisher.

Lee M and Penzien J (1983) Stochastic analysis of structures and piping systems subjected to stationary support excitations. *Earthquake Engineering & Structural Dynamics* 11: 91–110.

Lopez O, Hernandez J, Bonilla R and Fernandez A (2006) Response spectra for multicomponent structural analysis. *Earthquake Spectra* 22: 85–113.

Lou L and Zerva A (2004) Effects of spatially variable ground motions on the seismic response of a skewed, multi-span, RC highway bridge. *Soil Dynamics and Earthquake Engineering* 25: 729–740.

Luco J and Wong H (1986) Response of a rigid foundation to a spatially random ground motion. *Earthquake Engineering & Structural Dynamics* 14: 891–908.

Nazmy A and Abdel-Ghaffar A (1992) Effects of ground motion spatial variability on the response of cable-stayed bridges. *Earthquake Engineering & Structural Dynamics* 21: 1–20.

Papadopoulos S, Sextos A, Kwon O, Gerasimidis S and Deodatis G (2017) Impact of spatial variability of earthquake ground motion on seismic demand to natural gas transmission pipelines. In: *Proccedings of the 16th World Conference on Earthquake, 16WCEE 2017*. Santiago, Chile.

Priestley M, Seible F and Calvi G (1996) *Seismic design and retrofit of bridges*. John Wiley & Sons Ltd.

Rathje E, Abrahamson N and Bray J (1998) Simplified frequency content estimates of earthquake ground motions. *Journal of Geotechnical and Geoenvironmental Engineering* 124: 150–159.

Sextos A and Kappos A (2009) Evaluation of seismic response of bridges under asynchronous excitation and comparisons with Eurocode 8-2 provisions. *Bulletin of Earthquake Engineering* 7: 519–545.

Sextos A, Kappos A and Mergos P (2004) Effect of soil-structure interaction and spatial variability of ground motions on irregular bridges: The case of the Krystallopigi Bridge. In: *13th World Conference on Earthquake Engineering*. Vancouver (B.C. Canada).

Sextos A, Karakostas C, Lekidis V and Papadopoulos S (2014) Multiple support seismic excitation of the Evripos Bridge based on free-field and on-structure recordings. *Structure and Infrastructure Engineering* 11: 1510–1523.

Sextos A, Pitilakis K and Kappos A (2003) Inelastic dynamic analysis of RC bridges accounting for spatial variability of ground motion, site effects and soil–structure interaction phenomena. Part 1: Methodology and analytical tools. *Earthquake Engineering & Structural Dynamics* 32(4): 607–627.

Shinozuka M, Saxena V and Deodatis G (2000) Effect of spatial variation of ground on highway structures. Technical report, MCEER ISN 1520-295X.

790 Soyluk K and Dumanoglu A (2000) Comparison of asynchronous and stochastic dynamic
791 responses of a cable-stayed bridge. *Engineering Structures* 22: 435–445.
792 Soyluk K and Dumanoglu A (2004) Spatial variability effects of ground motions on cable-stayed
793 bridges. *Soil Dynamics and Earthquake Engineering* 24: 241–250.
794 Spudich P and Cranswick E (1984) Direct observation of rupture propagation during the 1979
795 Imperial Valley earthquake using a short baseline accelerometer array. *Bulletin of the*
796 *Seismological Society of America* 74: 2083–2114.
797 Tzanetos N, Elnashai A, Hamdan F and Antoniou S (2000) Inelastic dynamic response of RC
798 bridges subjected to spatial non-synchronous earthquake motion. *Advances in Structural*
799 *Engineering* 3: 191–214.
800 Wang J, Carr A, Cooke N and Moss P (2003) Wave-passage effect on the seismic response of long
801 bridges. In: *2003 Pacific Conference on Earthquake Engineering*.
802 Zerva A (1990) Response of multi-span beams to spatially incoherent seismic ground motions.
803 *Earthquake Engineering & Structural Dynamics* 19: 819–832.
804 Zerva A (1991) Effect of spatial variability and propagation of seismic ground motions on the
805 response of multiply supported structures. *Probabilistic Engineering Mechanics* 6: 212–221.
806 Zerva A (2009) *Spatial variation of seismic ground motions: Modeling and engineering*
807 *applications*. Boca Raton: CRC Press.